Geological Survey of Japan Cruise Report No. 18, p. 355–369, 1982

XVII. X-RAY DIFFRACTION STUDY OF MANGANESE NODULES AND ASSOCIATED ROCKS: THE WAKE TO TAHITI TRANSECT

Akira Usui

Introduction

X-ray powder diffraction analyses were made on manganese nodules and rocks from 51 stations along two traverses Lines A and B. The objectives are to observe the general trend of distribution of manganese and associated minerals and to reconfirm the relationship between the nodule surface structure and the mineral composition established in the previous cruise areas of the northern Central Pacific Basin. This X-ray diffraction analysis is a part of a petrological study including microscopical and microprobe analyses. This article describes the results of semiquantitative analysis for bulk powder samples.

Mineralogy of marine manganese minerals are still controversial because of their low crystallinity and small size as summarized by BURNS and BURNS (1977), and several mineral names have been reported for same minerals of nodules. USUI (1979) precisely characterized the nodule minerals and attributed 10 Å manganate (ARRHENIUS *et al.*, 1979), todorokite (BURNS and BURNS, 1977), and buserite (GIOVANOLI, 1979) to the 10 Å manganite phase, and birnessite (BURNS and BURNS, 1977) and vernadite (CHUKUROV *et al.* (1976)) to the δ-MnO_2 phase. The occurrence of marine 7 Å manganite (BUSER and GRÜTTER, 1956), often identified to terrestrial birnessite or ordered δ-MnO_2 is much limited. Its occurrence in deep-sea manganese nodules is doubtful, because 10 Å manganite easily changes to 7 Å manganite through dehydration and because the strong reflection of phillipsite at 7 Å is apt to be misinterpreted as that of manganese minerals. Accordingly, it is my opinion that the principal manganese mineral phase comprises a relatively well-crystalline and chemically homogeneous 10 Å manganite phase and a poorly crystalline δ-MnO_2 (2 line form) phase.

Sample preparation and analytical methods

Ferromanganese oxide layers separated from individual nodules from most of all stations, were dried at a room temperature. Sampling locations and nodule descriptions are summarized in Chapter VII (Appendix VII-2 and Fig. VII-7; USUI, this cruise report). Manganese materials were also removed from the rock samples and nodule nuclei. The X-ray powder diffraction was conducted in the constant measurement conditions using the Rotaflex RAD-rA (Rigaku Denki Co. Ltd.) with a monochrometer. Powder samples were mounted in the standard glass holder and subjected to nickel-filtered copper radiation (at 40 kV, 160 mA) during 8°(2θ)/min scan from 3° to 45° (2θ).

Identification of minerals is based on my previous method (USUI, 1979) and ASTM X-ray powder data files. It was extended to common marine minerals such as quartz, plagioclase(Ab–An), potash feldspars, olivine, calcite, zeolites, clay minerals, barite,

Table XVII-1 Relative mineral composition of manganese nodules.

Station no.	Sample no.	Nodule type	Relative abundance of constituents							Analyzed part
			manganese minerals		accessory minerals					
			T	D	Qtz	Plc	Ph	Mmt	others	
1590	B2(IN)	DPs+r	tr	×	××	×	××	—	—	inner, hard
	B2(OUT)	—	×	××	××	—	×	—	—	outer, upper side
	FG192–1	DPs	××	×	××	—	××	—	—	outer, bottom side
	FG192–2	DPs	××	×	××	tr	—	—	—	outer layers
1591	FG193–1	Sr	××	—	××	×	tr	—	—	whole nodule
	FG193–2	Sr	××	—	×	×	××	—	—	2 whole nodules
1592	FG194–1	IDs·r	××	tr	××	×	tr	—	—	whole nodule
1593	FG195–1	Ds·r	××	—	××	tr	××	tr	—	whole nodule
	FG195–2	Ds·r	××	tr	××	tr	tr	—	—	fragments
1594	FG196–1(IN)	IDPs	tr	××	××	×	×	×	—	inner
	FG196–1(OUT)	—	tr	×	×	—	—	—	—	outer layers
	FG196–3	IDPs	tr	××	××	×	×	tr	—	inner, hard
	FG196–4(IN)	IDPs+r	tr	××	×	—	×	—	—	inner, hard
	FG196–4(OUT)	—	×	×	×	tr	—	—	—	outer layers
1595	FG197–1	IDPs+r	××	×	××	—	tr	×	—	outer, bottom side
	FG197–3	IDPs	×	×	××	tr	—	—	K-fsp?	outer
1596	FG198–1	IDPs	tr	××	××	—	—	—	—	outer layer, top side
	FG198–3	IDPs	tr	×	××	×	—	—	—	outer 2 mm layer
1597	FG199–2	Sr	××	tr	××	×	×	—	—	whole nodule
1598	FG200–2	Sr	××	—	×××	×	—	×	—	surrounding layers
1599	FG201–2	Sr	×	×	×	—	×	—	—	surrounding layers
1600	FG202–2	Sr	××	—	×	—	××	—	—	whole nodule
1601	B6	Sr	×××	—	××	×	—	—	—	whole nodule
	FG203–1	Sr	××	—	××	tr	—	—	—	whole nodule
1603	FG205–2	Vr	××	—	××	×	—	—	—	whole nodule
1604	FG206–2	Vr	××	tr	××	×	—	—	—	surrounding layers
1606	B9(IN)	DPs	—	×	××	×	×	—	—	inner
	B9(OUT)	—	×	tr	×	×	—	—	—	outer
	FG208–2	Sr	××	—	×	×	—	tr	—	2 whole nodules
1607	FG209–1	IDPs	×	×	tr	×	××	—	—	fragments
1608	FG210–2	DPs	×	tr	×	×	××	—	—	fragments

Table XVII-1 (Continued)

Station no.	Sample no.	Nodule type	Relative abundance of constituents							Analyzed part
			manganese minerals		accessory minerals					
			T	D	Qtz	Plc	Ph	Mmt	others	
1609	FG211–1	DPs	—	×	—	tr	—	×	—	whole nodule
	FG211–2	DPs	—	×	—	—	—	—	—	fragments
1611	B11	Vs	×	—	—	—	××	—	—	whole nodule
1616	B14(IN)	Ss	tr	tr	××	×	—	tr	—	inner
	B14(LOW)	—	××	×	×	×	××	—	—	bottom side, microbotryoidal
	FG218–2	Ss	×	×	×	×	—	tr	K-fsp?	fragments
1617	B15(IN)	Ss	tr	×	×	×	tr	—	—	inner
	B15(LOW)	—	—	×	×	tr	—	—	—	bottom side, microbotryoidal
	FG219–2(IN)	Ss/Ds	tr	×	×	×	×	—	—	inner
	FG219–2(OUT)	—	tr	×	tr	tr	—	—	—	outer
1618	B16	Is	××	×	×	×	××	—	—	coalescent nodules
	FG220–2	Is	××	tr	×	×	××	—	—	coalescent nodules
1618A	FG221–1	Is	×	×	×	tr	×	—	—	coalescent nodules
1619	B17	DPs	×	tr	×	×	×	—	—	outer
	FG222–1	DPs	×	×	×	×	×	—	—	fragments
1620	B18	Ds	×	×	×	—	××	—	—	surrounding layers
	FG223–2	Ss	×	×	×	×	×	—	—	fragments
1621	B19	Ss	×	×	×	×	—	—	—	fragments
	FG224–2	DPs	×	×	×	tr	tr	—	—	fragments
1622	FG225–1	Ss	××	×	×	×	×	—	—	fragments
1623	B20	Ss	—	××	tr	—	tr	—	—	fragments
	B20X	Ss	—	××	—	tr	—	—	—	fragments
1625	B21	Ss/Ds	×	×	××	××	×	×	—	2 whole nodules
	FG228–1	Ss	×	×	×	××	××	—	—	3 whole nodules
1627	B22	Sr	××	tr	××	××	××	—	—	whole nodule
1628	FG231–2	Ir	×××	—	×	×	—	—	—	half of nodule
1629	B23	Sr	××	tr	××	×	×	—	—	fragments
	FG232–1	Sr	×××	—	×	×	×	—	—	2 whole nodules
1630	FG233–1	Sr	××	tr	××	××	—	×	—	whole nodule
1631	B24	Sr	××	tr	×	×	—	—	—	whole nodule
	FG234–1	SPs·r	××	tr	×	×	—	tr	—	whole nodule

Table XVII-1 (Continued)

Station no.	Sample no.	Nodule type	Relative abundance of constituents							Analyzed part
			manganese minerals			accessory minerals				
			T	D	Qtz	Plc	Ph	Mmt	others	
1632	FG235-2	Sr?	—	×	—	××	—	—	—	coating of pumice
1634	FG237-1	IDPs·r	×	×	×	×	—	—	—	fragments
1635	B26	Sr	×××	—	××	—	—	tr	—	half of nodule
	FG238-1	Sr	×××	—	××	—	—	—	—	whole nodule
1635A	FG239-1	IDPs·r	××	×	×	—	—	—	—	fragments
1636	FG240-1	Vr	×××	—	××	×	—	—	—	whole nodule
1638	FG242-2	Sr	××	tr	××	tr	—	tr	—	half of nodule
1639	B28	Sr	×××	—	××	—	—	—	—	whole nodule
	FG243-1	Sr	×××	—	××	×	—	—	—	whole nodule
1640	FG244-1	Sr	××	—	××	×	—	tr	—	whole nodule
1641	B29	Sr	××	tr	××	×	—	—	—	half of nodule
	FG245-1	Sr	××	tr	××	tr	tr	—	—	fragments
1642	FG246-1	IDPs	×	×	××	×	tr	tr	K-fsp?	fragments
1643	FG247-1	IDPs	×	××	××	×	tr	—	—	fragments
1644	FG248-2	SPs+r	×	×	××	×	×	—	—	fragments
1645	B30(IN)	Ds	—	××	××	×	tr	—	—	inner
	B30(OUT)	—	—	××	××	—	tr?	—	—	outer 2 mm layers
	FG249-1	DPs	×	××	×	—	×	—	—	fragments
1646	B31	Ds	××	×	××	—	××	—	—	2 whole nodules
	FG250-2	DPs	×	××	××	tr	××	—	—	3 whole nodules
1647	B32(IN)	Ds	—	××	××	×	×	—	—	inner
	B32(OUT)	—	—	××	××	—	—	—	—	outer layers
	FG251-1	Ds	×	××	××	—	×	—	—	outer layers

Notes. T: 10 Å manganite, D: δ-MnO_2, Qtz: quartz, Plc: plagioclase, Ph: phillipsite, Mmt: montmorillonite, K-fsp: orhtoclase or microcline, ×××: abundant, ××: common, ×: present, tr: trace, —: not detected.

Table XVII-2 Relative mineral composition of rocks from sediment surface.

Station no.	Sample no.	Relative abundance of constituents								External features
		Qtz	FSP		ZLT		Mmt	Ap	others	
			Plc	Kfsp	Ph	Cp				
1590	FG192-2	××	—	—	tr	—	tr	—	—	hard white plate
1593	FG195-1	××	—	—	—	—	tr	—	—	hard yellowish white plate
	FG195-2a	××	—	—	—	—	tr	—	—	do.
	FG195-2b	××	—	—	tr	—	tr	—	—	do.
1594	FG196-3a	××	—	—	tr	—	tr	—	—	translucent rock fragment
	FG196-3b	×	tr	—	×	tr	tr	—	—	thin brown coating of nodules
1595	FG197-3	tr	tr	×	—	—	×	—	magnetite	soft yellowish brown rock (Mn coating)
1596	FG198-1	tr	—	tr	—	—	×	—	—	angular faceted brown rock
1599	FG201-2	tr	—	—	×××	—	×	×	—	irregular yellowish borwn rock (Mn coating)
	FG201-3	—	—	—	×	—	×	—	kaolinite?	do.
	FG201-4	tr	—	—	×	—	×	—	illite?	do.
	FG201-5	tr	—	—	×	—	×	—	—	do.
1603	FG205-2	tr	—	—	—	—	—	×	—	do.
1608	FG210-2	—	—	—	—	—	××	—	—	angular yellowish brown rock (Mn coating)
1611	FG213-1	tr	—	—	×××	—	—	—	—	hard white rock (do.)
1616	FG218-2	tr	—	—	×	—	×	—	—	stacked thin layers (Mn coating)
1618	B16	—	tr	—	××	—	tr	—	—	brown irregular aggregate
	FG220-1	tr	—	—	××	—	tr	—	—	do.
	FG220-2	tr	—	—	×	—	—	—	—	do.
1618A	FG221-1	tr	—	—	×××	—	tr	—	—	white plate
	FG221-2	tr	—	—	××	—	×	—	—	white plate and brown rock fragment
1619	B17	×	—	—	×	×	—	—	—	irregular brown rock fragment
	FG222-1	tr	—	—	××	—	tr	—	—	brown plate
1620	B18	××	—	—	—	—	—	—	—	translucent rock fragment
1625	B21a	tr	tr	tr	×××	—	×	—	—	hard brown irregular aggregate
	B21b	tr	tr	—	×	—	×	×	—	granular gray rock fragment
	FG228-1	tr	tr	—	××	—	tr	—	—	yellowish brown plate (Mn coating)
	FG228-2	tr	tr	—	×××	—	tr	—	—	yellowish brown irregular aggregate
1629	B23	—	—	—	×××	×	tr	—	—	white pipe of 3 mm diameter (Mn coating)
	FG232-1	tr	—	—	×××	—	tr	—	—	brown and white rock fragment (do.)
1631	B24	tr	—	—	—	—	tr	—	—	thin buff coating of nodules

Table XVII-2 (Continued)

Station no.	Sample no.	Relative abundance of constituents								External features
		Qtz	FSP		ZLT		Mmt	Ap	others	
			Plc	Kfsp	Ph	Cp				
1635	FG239–2	×	×	—	—	—	××	—	—	yellowish brown rock fragment (Mn coating)
1642	FG246–1	×	tr	—	×	—	×	—	—	clay filling cracks
1644	FG248–1	tr	××	—	—	—	×	—	—	yellowish brown pebble (Mn coating)
	FG248–2	tr	××	tr	tr	—	×	—	—	granular gray pebble (Mn coating)
1645	FG249–2	××	tr	—	×	—	×	—	kaolinite?	clay filling cracks
1646	B31	××	—	—	—	—	×	—	—	hard white plate (Mn coating)
	FG250–1	××	—	—	×	—	×	—	—	yellowish brown plate (Mn coating)
	FG250–2	××	tr	—	tr	—	tr	—	—	soft white aggregate within nodules

Notes, FSP: feldspars, ZLT: zeolites, Cp: clinoptilolite, Ap: apatite.

Table XVII-3 Relative mineral composition of nodule nuclei.

Station no.	Sample no.	Relative abundance of constituents							External features
		Qtz	FSP		ZLT		Mmt	Ap	
			Plc	Kfsp	Ph	Cp			
1590	FG192–1	××	—	—	×××	—	—	—	hard white plate
	FG192–2	××	—	—	—	—	×	—	do.
1594	FG196–1	××	tr	—	×	—	×	—	soft white pebble
1595	FG197–1	tr	—	—	×	×	×	—	soft white rock fragment
	FG197–2	××	—	—	—	×	××	—	do.
	FG197–3	tr	—	×	—	—	××	—	do.
	FG197–4	tr	tr	×	×	—	××	—	soft yellowish white rock fragment
1596	FG198–2	tr	tr	×	—	—	×	—	do.
	FG198–3	tr	tr	—	tr	—	×	—	yellowish brown rock fragment
	FG198–4	tr	—	×	—	—	××	—	do.
1597	FG199–1	tr	—	—	×	—	××	—	do.
	FG199–2	×	—	—	××	—	××	—	yellowish white rock fragment
1604	FG206–2	tr	×	—	—	—	—	—	grayish white rock fragment
1607	FG209–1	—	—	—	××	××	tr	—	soft yellowish brown rock fragment
1609	FG211–2	—	—	×	—	—	×	×	white and brown rock fragments
1611	B11	—	—	—	×××	—	—	—	hard white irregular aggregate
1619	FG222–1	tr	tr	—	××	—	—	—	soft white rock fragment
	FG222–2	tr	×	—	××	—	—	—	do.
1620	FG223–1	××	—	—	—	—	—	—	hard translucent rock fragment
	FG223–2	××	—	—	—	—	—	—	do.
1621	B19	×	—	tr	×	—	×	—	soft yellowish brown rock fragment
	FG224–1	×	—	×	××	—	×	—	yellowish white rock fragment
1622	FG225–1	tr	—	—	×××	—	tr	×	do.
1623	B20	tr	×	—	×××	—	tr	—	soft yellowish brown rock fragment
	B20X	tr	×	×	—	××	×	—	yellowish white rock fragment
1629	B23	×	—	—	×	—	×	—	do.
1635A	FG239–1	×	—	—	tr	—	tr	—	soft white rock fragment
1640	FG244–1	—	—	—	—	××	tr	—	white plate
1641	B29	×	×	—	×	—	tr	—	translucent rock fragment

apatite, goethite, aragonite, magnetite, hematite, celestite, cristobalite, and others.

Determination of constituent minerals

The results of identification are summarized in Tables XVII-1 to 3. The intensity of X-ray reflection principally indicates the relative amount of constituent mineral. The peak heights at a diagnostic *d* value were measured, and the relative abundance was tentatively graded from "tr" to "×××" in the tables. The symbol "tr" in the tables means indefinite determination based on only one or two weak reflections.

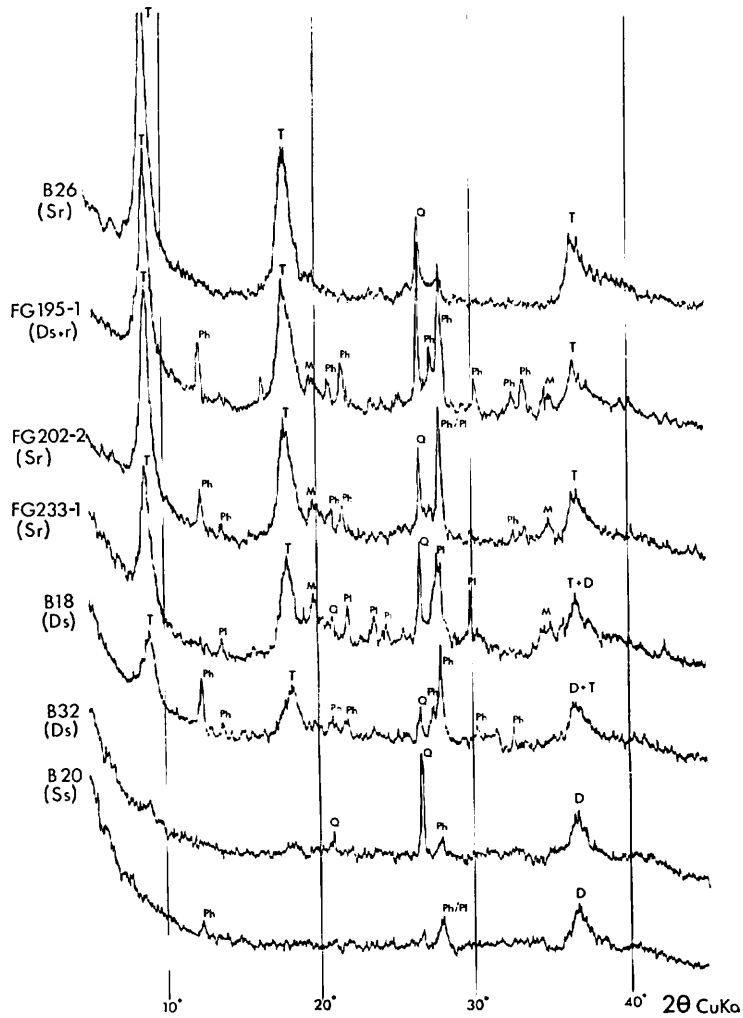

Fig. XVII-1 Typical X-ray powder diffraction patterns of manganese nodules. Symbols in parentheses are nodule morphological types (see in Chapter VII). T: 10 Å manganite, D: δ-MnO_2 (2 line form), Q: quartz, Pl: plagioclase, Ph: phillipsite, M: montmorillonite, T+D; D+T: the reflection of the former is stronger.

Definitely identified mineral species are 10 Å manganite, 2 line form δ-MnO_2, quartz, palgioclase(oligoclase-labradorite), phillipsite, (or harmotome), and montmorillonite in nodule oxide layers. Quartz, plagioclase, phillipsite, clinoptilolite, potash feldspar (orthoclase and/or microcline), montmorillonite, apatite, and magnetite (only in one sample) were determined in nodule nuclei and associated rocks. Other clay minerals, kaolinite and illite, may be present in rocks.

The relative abundance of minerals in nodules is summarized in Table XVII-1, and typical X-ray powder patterns of manganese minerals are shown in Fig. XVII-1. Iron oxide minerals were not identifiable despite the presence of 5–10% iron in nodules (USUI and MOCHIZUKI, this cruise report). Iron is considered to be concentrated mainly as amorphous ferric oxide (BURNS and BURNS, 1979) in the δ-MnO_2 phase (USUI, 1979).

Manganese oxide minerals determined as nodule constituents are 10 Å manganite and 2 line form δ-MnO_2 (abbr.: δ-MnO_2) for the nodules studied, and 7 Å manganite were not detected. A sharp peak at about 7 Å occasionally found can be attributed to phillipsite because other strong reflections corresponding to phillipsite are always present when the 7 Å reflection exists. The X-ray pattern of 10 Å manganite is characterized by the reflections at 10, 5.0, 2.4, and 1.4 Å, while δ-MnO_2 by reflections at 2.4 and 1.4 Å. The relative abundance of 10 Å manganite was determined according to the peak height at 10 Å. The amount of δ-MnO_2 can not be directly evaluated from the height at 2.4 Å

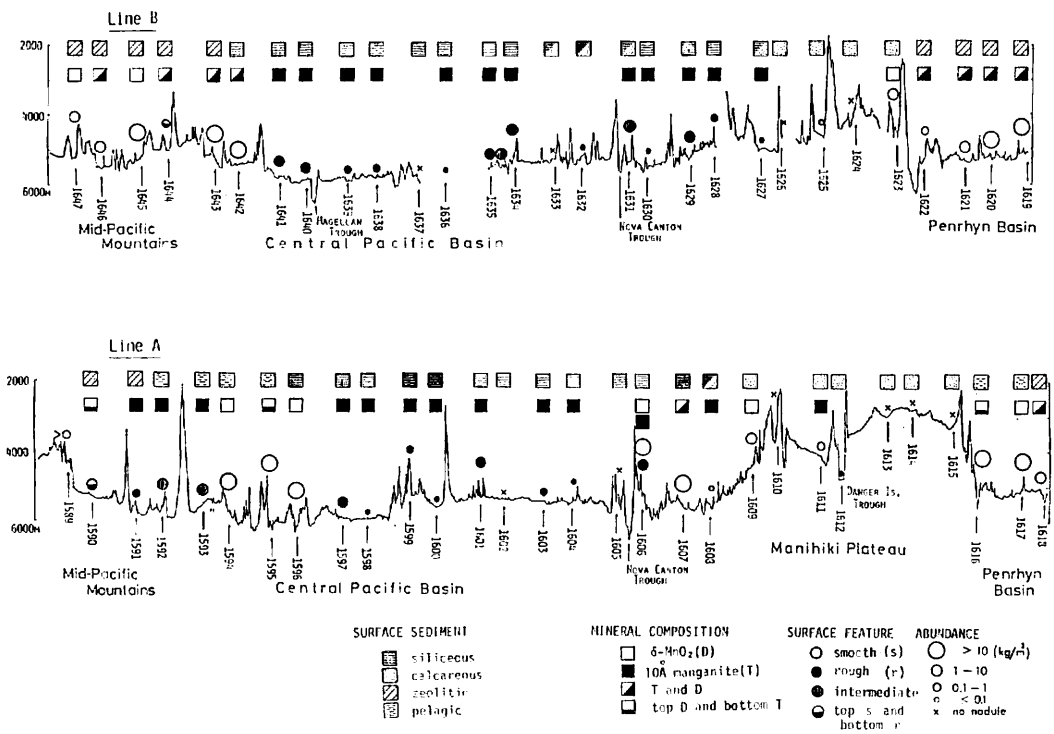

Fig. XVII-2 Regional variation of relative mineral composition of manganese nodules, showing correlations of mineral composition with nodule surface feature and associated sediment type.

because the reflection is responsible for the both minerals. The relative abundance was estimated from the peak heights at 10 Å and 2.4 Å on the assumption that the peak height ratio of the marine 10 Å manganite at 10 Å and 2.4 Å is 7.0 (USUI, unpublished data). Therefore the estimation of δ-MnO_2 is less reliable than that of 10 Å manganite. It should be also noted that the absolute contents of the two minerals in the bulk powder sample are unknown from these data and that the amount of 10 Å manganite is apt to be overestimated because of its better crystallinity.

Distribution of manganese minerals

The mode of occurrence and external and internal morphology of nodules are significantly variable along the traverses as are described in detail in Chapter VII (USUI, this cruise report). The X-ray diffraction analysis has revealed a marked correlation between nodule surface texture and manganese mineral composition (Fig. XVII-2).

Rough type nodules are distributed almost exclusively in the central to southern part of the Central Pacific Basin except for the vicinity of the Nova-Canton Trough where s-type nodules are locally distributed. Gritty surface of r-type nodules is composed of a thin layer of the 10 Å manganite phase. The 10 Å manganite layers dominate also inside the nodules but the δ-MnO_2 phase is rare (Table XVII-1 and Appendix VII-2). The gritty surface which is always composed of 10 Å manganite often develops on the

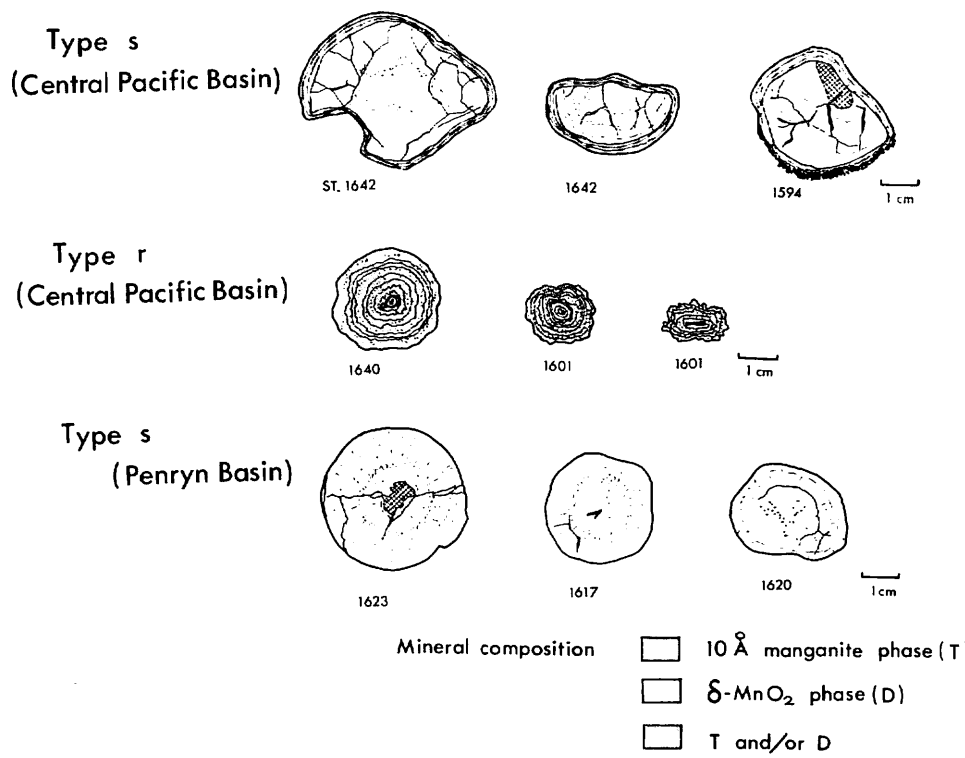

Fig. XVII-3 Schematic illustration of nodule sections and mineral compositions of typical manganese nodules.

bottom surface of smooth type nodules from the northern part of the traverses (Sts. 1590, 1595, 1644). It is noticed that the regional distribution of 10 Å manganite in type r and in the bottom of type s+r is markedly correlated with the distribution of siliceous ooze/clay as surface sediment. The fact suggests the close relationship of the deposition of 10 Å manganite to the diagenesis of siliceous sediments.

On the other hand, smooth type nodules from the Mid-Pacific Mountain area and the northern part of the Central Pacific Basin include the internal older nodules, usually fragmented, surrounded by thin layers. The mineral constituent of the internal older nodules is exclusively δ-MnO_2, while those of the surrounding layers are dominantly δ-MnO_2, with minor amounts of 10 Å manganite (Fig. XVII-3). Pelagic or zeolitic clay is dominant in the regions where type s is distributed.

As stated, the mineralogical characteristics of the nodules from the Central Pacific Basin and the Mid-Pacific Mountains area are compatible to our previous observations. However, the Penrhyn Basin nodules are somewhat different from the Central Pacific Basin nodules in mineralogical characteristics.

The nodules from the Penrhyn Basin are mostly spherical to discoidal and often fragmented, and the principal mineral constituent is δ-MnO_2. The conclusion is correspondent to the previous reports on the South and Central Pacific nodules by the New Zealand scientists (BÄCKER *et al.*, 1976; MEYLAN *et al.*, 1978). However, it is noted that 10 Å manganite is occasionally detected despite the absence of typical gritty structure in the nodules. 10 Å manganite is found in the irregular or small spherical nodules from six stations in this basin (Table XVII-1 and Appendix VII-2). Moreover, significantly high Mn/Fe and (Cu+Ni+Zn)/Mn (USUI and MOCHIZUKI, this cruise report) are locally found (Sts. 1618, 1622) among the stations. These facts suggest the possibilities that the 10 Å manganite develops in the interior of nodules, for instance, as massive or clastic structure, and that the growth mechanism of 10 Å manganite in the Penrhyn Basin nodules are different from that of the Central Pacific Basin.

Such peculiar feature is not explainable simply based on the X-ray diffraction study. Microscopical and microprobe analyses are needed to elucidate the growth process of the nodules and the mode of development of the individual mineral phases.

Accessory minerals in manganese nodules and associated rocks

Several detrital and authigenic accessory minerals were identified on the basis of bulk analysis of ferromanganese oxide layers, nuclei, and associated rocks (Tables XVII-2, -3). Typical X-ray powder patterns are shown in Fig. XVII-4. Quartz, plagioclase, and montmorillonite are most commonly distributed in the ferromanganese oxide layers. Quartz and plagioclase, microscopic in size, are probably incorporated as detrital particles during the growth of manganese minerals. Montmorillonite is not dominant in the oxide layer, except as a constituent of filling material of nodule internal cracks.

Various consolidated rocks as large as a few centimeters, found in the surface sediment and as nodule nuclei, are composed of quartz, feldspars, zeolites, clay minerals, and apatite. Regional occurrence of the mineral are shown in Fig. XVII-5.

White or transluscent rock fragments of chert are distributed in the northern part of the Central Pacific Basin, the Mid-Pacific Mountains (Sts. 1590, 1593, 1594, 1646), and the Penrhyn Basin (St. 1620). The chert fragments are preferentially distributed in the area

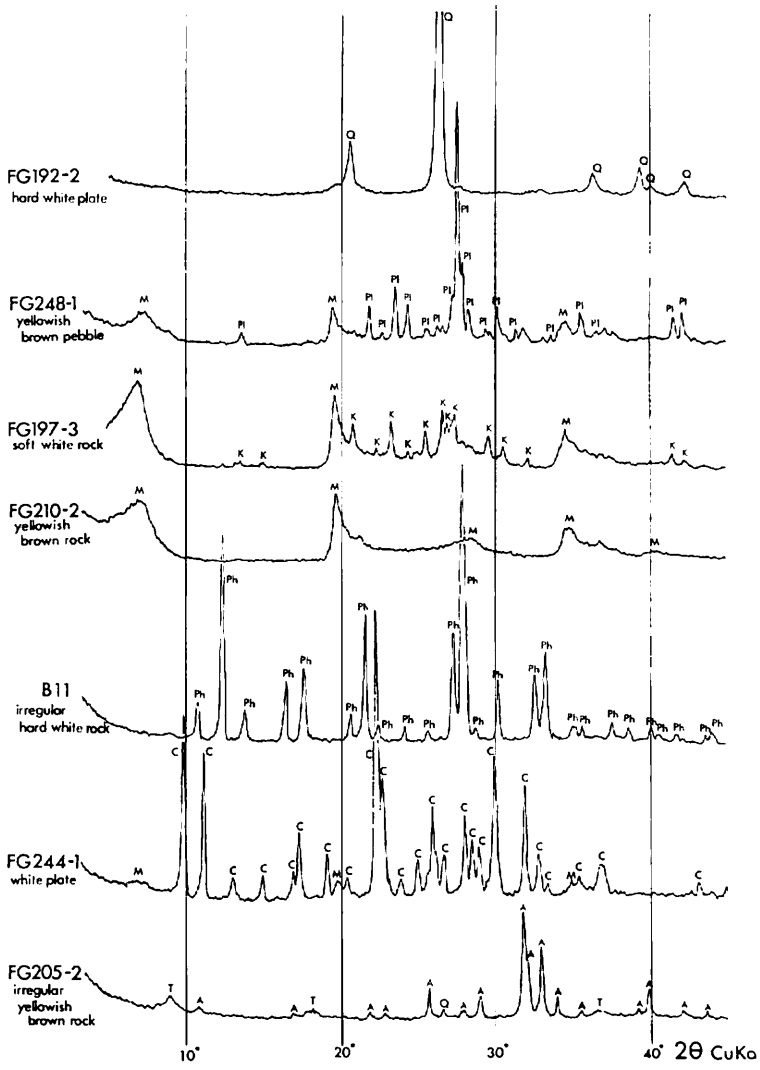

Fig. XVII-4 Typical X-ray powder patterns of rocks and nodule nuclei. K: orthoclase or microcline, C: clinoptilolite, A: apatite, others: see Fig. XVII-1.

where the s-type nodules (δ-MnO_2 rich) dominate, but rare in the Central Pacific Basin where siliceous sediments and r-type nodules (10 Å manganite rich) dominate. The fact may be related to the age of formation of the nodules, if the chert fragments represents the older age of formation.

Soft, yellowish brown to white rocks variable in shape (platy, angular, and irregular) are most abundant on these traverses. Montmorillonite and/or phillipsite are the major constituents of these rocks. It seems that the mode of distribution of the rocks has no remarkable relationship to the geological provinces or manganese nodule deposits, though the two minerals are scarce in the central part of the Central Pacific Basin except at St. 1635. Basaltic glass is considered to be as precursor of marine phillipsite and

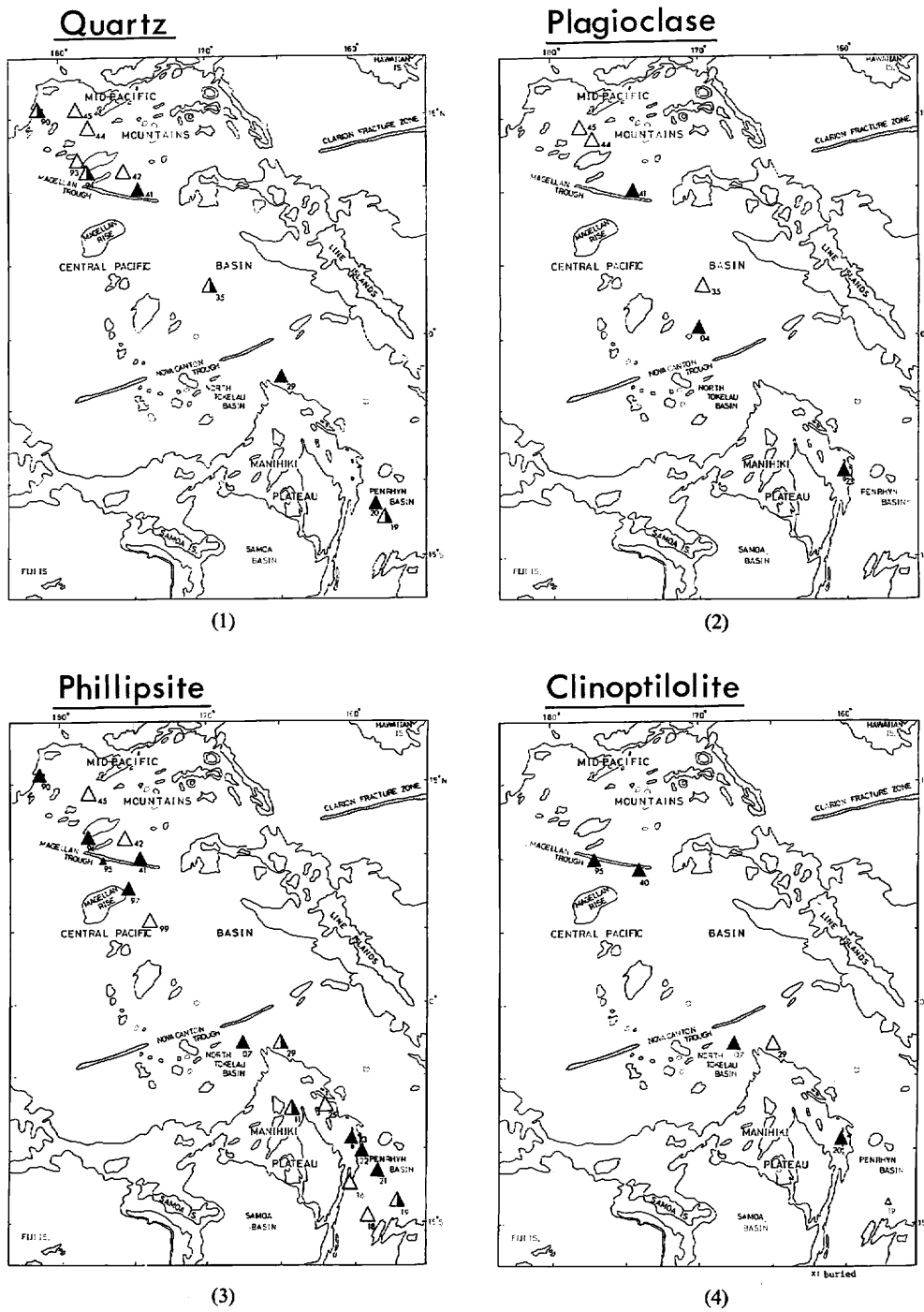

Fig. XVII-5 Regional occurrence of constituent minerals of rocks from sediment surface and nodule nuclei. 1) solid: in nodule nuclei, 2) open: in rocks other than nodule nuclei, 3) half solid: both in nuclei and rocks. Station number is shown by the last two digits; e.g., 95 means St. 1595 and 09 means St. 1609.

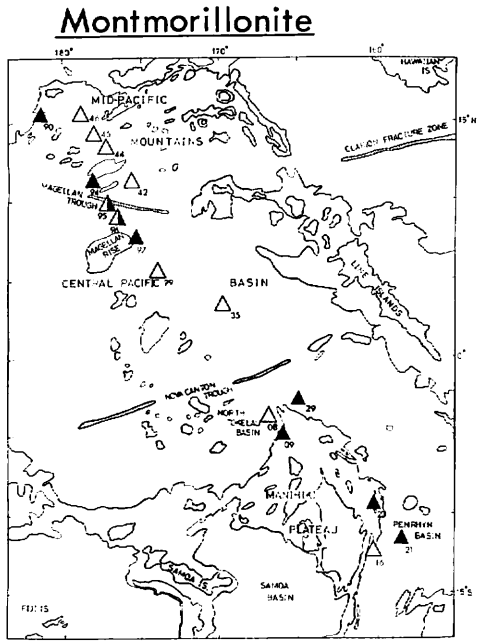

(5)

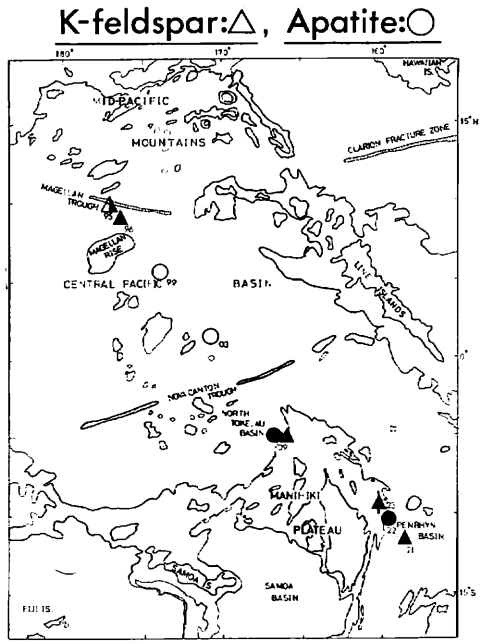

(6)

montmorillonite. HONNOREZ (1978) concluded that submarine alteration of basaltic glass at low temperature results principally in the formation of phillipsites, smectites, and Fe–Mn oxides in various stages of palagonitization. The rocks collected in this area are presumably identifiable as palagonitized glasses in various stages.

Potash feldspars, identified to orthoclase or microcline, were found from several stations by means of X-ray analysis (Sts. 1595, 1596, 1609, 1621, 1623). Occurrence of potash feldspar has been reported in the DSDP cores from the Line Island (KELTS and MCKENZIE, 1976) situated 200 km apart eastward of the Line B. The DSDP potash feldspar (intermediate microcline) is believed to be a diagenetic product from the interstitial water of the Cretaceous volcanic sediments. Microscopic study and comparative geological study may provide a similar origin of the potash feldspar from this area.

Clinoptilolite occurs mainly in the nodule nuclei from several stations. It is not found in the rocks in surface sediments, though exceptionally traced in the phillipsite rich rocks from St. 1629. This occurrence is consistent with the conception that marine clinoptilolite occurs in the older sediments than phillipsite and is a diagenetic product after burial (BOLES and WISE, 1978). However, it is difficult to conclude only from this result that the age of initial formation of nodules with clinoptilolite nuclei is relatively old.

Apatite was detected mainly in yellowish rock of nodule nuclei (Sts. 1609, 1622) and in the rocks in sediment surface (St. 1599). However, we have no available data suggesting its organic or inorganic origin.

Magnetite was detected in a soft yellowish rock which appears palagonitized glass (St. 1595).

Finally it is stressed that the precise microscopic and geochemical investigation of manganese nodules should be followed to this study which have outlined the mineral composition of manganese nodules.

References

ARRHENIUS, G., CHEUNG, K., CRANE, S., FISK, M., FRAZER, J., KORKISCH, J., MELLIN, T., NAKAO, S., TSAI, A., and WOLF, G. (1979) Counterions in marine manganates. *La Genèse des Nodules de Manganèse, Colloq. Intl. C. N. R. S.*, no. 289, p. 333–356.

BÄCKER, H., GLASBY, G. P., and MEYLAN, M. A. (1976) Manganese nodules from the Southwestern Pacific Basin. *N.Z.O.I. Oceanogr. Field Rept.*, no. 6, 88p.

BOLES, J. R. and WISE, W. S. (1978) Nature and origin of deep-sea clinoptilolite. *In* SAND, L. B. and MUMPTON, F. A. (*eds.*), *Natural Zeolites, Occurrence, Properties, Use*, Pergamon press, p. 235–243.

BURNS, R. G. and BURNS, V. M. (1977) Mineralogy of manganese nodules. *In* GLASBY, G. P. (*ed.*), *Marine Manganese Deposits*, Elsevier, New York, p. 185–248.

——— and ——— (1979) Manganese oxides. *In* Burns, R. C. (*ed.*), *Marine Minerals*, Miner. Soc. Amer. Short Course Notes, vol. 6, p. 1–46.

BUSER, W. and GRÜTTER, A. (1956) Über die Natur der Manganknollen. *Schweiz. Min. Petr. Mitt.*, vol. 36, p. 49–62.

CHUKHROV, G. V., ZVYAGIN, B. B., YERMILOVA, L. P., and GORSHKOV, A. J. (1976) Mineralogical criteria in the origin of marine iron-manganese nodules. *Mineral. Deposita*, vol. 11, p. 24–32.

GIOVANOLI, R. (1979) On natural and synthetic manganese nodules. *In* VARENTSOV, I. (*ed.*), *Geology and Geochemistry of Manganese*, Hungarian Acad. Sci. Publ., p. 159–202.

HONNORENZ, J. (1978) Generation of phillipsites by palagonitization of basaltic glass in sea water and the origin of K-rich deep-sea sediments. *In* Sand, L. B. and MUMPTON, F. A. (*eds.*), *Natural Zeolites, Occurrence Properties, Use*, Pergamon Press, p. 245–258.

KELTS, K. and MCKENZIE, J. A. (1976) Cretaceous volcanogenic sediments from the Line Island Chain: Diagenesis and formation of K-feldspar, DSDP Leg 33, Hole 315A and site 316. *In* SCHLANGER, S. O., JACKSON, E. D., *et al., Init. Repts. DSDP*, vol. 33, Washington (U. S. Govt. Print. Office), p. 789–831.

MEYLAN, M. A., GLASBY, G. P., MCDOUGALL, J. C., and SINGLETON, R. J. (1978) Manganese Nodules and Associated Sediments froma- the Samoan Basin and Passage. *N.Z.O.I. Oceanogr. Field Rept.*, no. 11, 61p.

USUI, A. (1979) Minerals, metal contents, and mechanism of formation of manganese nodules from the Central Pacific Basin (GH76–1 and GH77–1 areas). *In* BISCHOFF, J. L. and PIPER, D. Z. (*eds.*), *Marine Geology and Oceanography of the Pacific Manganese Nodule Province*, Plenum Publ. Co., p. 651–679.